International Journal of Mechanical and Production Engineering Research and Development (IJMPERD)
ISSN(P): 2249-6890; ISSN(E): 2249-8001
Vol. 5, Issue 1, Feb 2015, 35-44

SIMULATION ANALYSIS OF FOUR-PASS SHAPE ROLL FORMING OF I-SECTIONS

A. CHENNAKESAVA REDDY

Professor, Department of Mechanical Engineering, JNTUH College of Engineering Kukatpally, Hyderabad, Andhra Pradesh, India

ABSTRACT

This paper presents the simulation of shape rolling of I-section using DEFORM software. The material is AA 2024. Four-pass shape rolling was adopted to obtain I-section. The flow stress and strain were within the limits of allowable stress and strain of AA2024 material. This paper provides the reference for the numerical simulation and application of cold rolled I- section beams.

KEYWORDS: Simulation; Shape Rolling, I-Section Beam, Four Pass, DEFORM

INTRODUCTION

Chennakesava (2012) evaluated of local thinning during cup drawing of gas cylinder steel using isotropic criteria using finite element method. Chennakesava (2006) employed finite element analysis for reverse superplastic blow forming of Ti-Al-4V alloy. He optimized the thickness variation using ABAQUS. Boljanovic et al (2009) studied the shape rolling process where structural shapes were passed through rollers to deform the workpiece to a desired shape while maintaining a constant cross-section. Structural shapes that can be rolled include: I-beams, H-beams, T-beams, U-beams, angle iron, channels, bar stock, and railroad rails. The rolls form the part to a specific shape. Shape rolling is the most economical, cost –competitive process to follow for a given component. Shape rolling cannot be done in one pass but multiple passes are required to get final shape. Most shape rolling involves passing the material through several passes. Many researchers of the cold roll forming process have investigated computer-aided design or numerical simulation of the cold roll forming process in order to manufacture products while increasing the productivity and maintaining the accuracy of the resulting products [Kiuch et al (1986); Onoda et al (1989); Duggal (1996)]. The mesh generation and remeshing has a higher degree of complexity in case of 3D finite element method simulation. Early attempts to perform 3D Fem simulations of different processes were using a mesh with brick elements [Heislitz et al (1996); Wu et al (1990)]. However, when the mesh was too distorted to continue the simulation it was necessary to remesh manually the deformed billet. This procedure is time consuming and error prone.

Therefore, the application for 3D problems is still not widely used in industry because it is not always cost effective and requires considerable engineering and computation time. In massive forming, simulation of 2D problems, e.g. axisymmetric and plane or near-plane strain, is truly state of the art. The present work involves the finite simulation of shape rolling of I-shaped structural component using DEFROM-2D.

YIELDING UNDER PLANE STRAIN CONDITIONS

The true stress-strain curve is called a flow curve because it gives the stress required to cause the metal to flow plastically to any given strain.

$$\sigma = K\varepsilon^n \quad \text{.} \quad \text{.... (1)}$$

where k is the stress at $\varepsilon = 1.0$ and n, the strain hardening exponent.

For plain strain conditions as shown in figure 1, $d\varepsilon_2 = 0$. If there is no volume change, $d\varepsilon_1 = -d\varepsilon_3$, assuming no elastic deformation. The deformation is pure shear strain. Therefore, yielding occurs in plain strain at the critical shear stress. Plane strain is applicable to rolling, drawing and forging where flow in a particular direction is constrained by the geometry of the machinery.

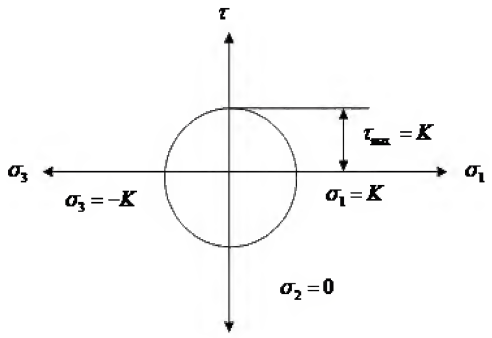

Figure 1: Yielding Under Plain Strain Conditions

Applying Tresca criterion,

$$\frac{\sigma_2 - \sigma_3}{2} = K = \frac{\sigma_y}{2} \quad \text{... (2)}$$

where K = shear yield stress and σ_y = uniaxial yield stress.

Applying von Mise's criterion,

$$(\sigma_1 - \sigma_2)^2 + (\sigma_2 - \sigma_3)^2 + (\sigma_3 - \sigma_1)^2 = 2\sigma_y^2 \quad \text{`. (3)}$$

$$K^2 + K^2 + 4K^2 = 2\sigma_y^2$$

$$2K = 1.1547\sigma_y \quad \text{... (4)}$$

where σ_1, σ_2, σ_3 are principal stresses, τ_{max} maximum shear stress, and σ_y yield stress.

Therefore, if the problem is of plane strain, the Tresca yield criterion and the von Mises yield criterion have the same result expressed in terms of K. It is unnecessary to specify which criterion used, provided the use of K.

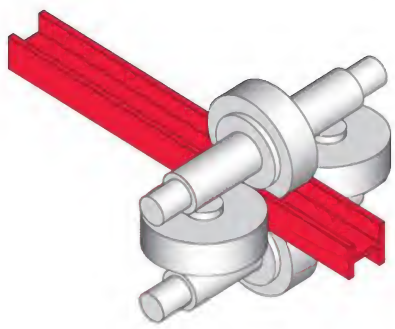

Figure 2: Rolling Process for I-Shaped Structural Component

METHODOLOGY

Finite element simulation can be utilized to analyze bulk metal forming process that can be represented by a plane strain or axis-symmetric deformation. The present work involves the finite simulation of shape rolling of I-shaped structural component. The rolling process for I-shaped structural component is shown in figure 2. This is modeled as plain strain deformation using DEFROM-2D. The material is 2024-T4. The chemical composition of AA 2024 aluminum alloy is given in table 1. The mechanical properties of AA 2024 are given in table 2. The initial geometry of upper roller, lower roller, left roller, right roller, and workpiece are given tables 3-7.

Table 1: Chemical Composition of AA2024

Component	Cu	Mg	Mn	Fe	Cr	Si	Ti	Zn	Al
Wt.%	4.0	1.4	0.4	Max 0.5	Max 0.1	Max 0.5	Max 0.15	Max 0.25	Balance

Table 2: Mechanical Properties of AA2024

S. No.	Property	Value	Unit
1	Ultimate tensile strength	469	MPa
2	Yield strength	324	MPa
3	Shear strength	283	MPa
4	Elongation	10	%
5	Hardness	120	BHN
6	Poisson's ratio	0.33	
7	Elastic modulus	73.1	GPa
8	Shear modulus	28	GPa
9	Strain hardening component	0.17	

Table 3: Initial Geometry of Upper Roller

S. No.	X	Y	R
1	0	2.95	0
2	1.4	2.95	0
3	1.6	2.75	0
4	1.6	2.35	0
5	1.9	2.35	0
6	2.1	2.75	0
7	2.3	2.75	0
8	2.5	2.35	0.1
9	3.2	2.35	0.1
10	3.4	2.75	0
11	3.6	2.75	0
12	3.8	2.35	0
13	4.1	2.35	0
14	4.3	2.95	0
15	5.7	2.95	0

Table 4: Initial Geometry of Lower Roller

S. No.	X	Y	R
1	5.7	0.5	0
2	4.3	0.5	0
3	4.1	1.2	0
4	3.8	1.2	0
5	3.6	0.7	0
6	3.4	0.7	0
7	3.2	1.2	0.1
8	2.5	1.2	0.1
9	2.3	0.7	0
10	2.1	0.7	0
11	1.9	1.2	0
12	1.6	1.2	0
13	1.6	0.7	0
14	1.4	0.5	0
15	0	0.5	0

Table 5: Initial Geometry of Right Roller

S. No.	X	Y	R
1	5.34	2.37	0
2	3.14	2.37	0
3	3.04	1.87	0
4	3.14	1.37	0
5	3.34	1.37	0

Table 6: Initial Geometry of Left Roller

S. No.	X	Y	R
1	-0.25	1.36	0
2	1.25	1.36	0
3	1.35	1.86	0
4	1.25	2.36	0
5	1.35	2.36	0

Table 7: Initial Geometry of Work piece

S. No.	X	Y	R
1	2.25	1.20	0
2	3.14	1.20	0
3	3.23	1.20	0
4	3.45	1.20	0
5	3.45	2.35	0
6	3.23	2.35	0
7	3.14	2.35	0
8	2.57	2.35	0
9	2.48	2.35	0
10	2.25	2.35	0
11	2.25	1.20	0

Initial settings before going to the simulation are:

- Speed for rollers: 0.1 mm/s
- Mesh generation: 200 nodes for workpiece and 400 for remaining 3 objects.
- Tolerance: 0.001

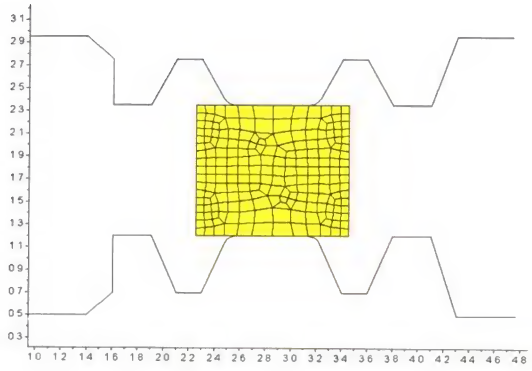

Figure 3: Initial Setups of Upper Roller, Lower Roller, and Work piece

Automatic mesh generation was used to mesh all objects. Continuous simulation of four passes was used for the present work. The initial setups for upper roller, lower roller and workpiece used for simulation of making I-section are shown in figure 3. After initial settings were completed, the simulation runs were conducted to process the work. While simulating the upper roller had translation movement downwards with a speed of 1mm/s and the lower roller had the translation movement upwards with a speed of 1mm/s. The deformed shape after first pass is shown in figure 4a. For second pass setup for simulation left and right rollers are introduced as shown in figure 4b. During simulation right roller moves leftward with a speed of 1mm/s and left roller moves rightward with a speed of 1mm/s. Upper and lower rollers remain same. The deformed shape after second pass is shown in figure 5a.

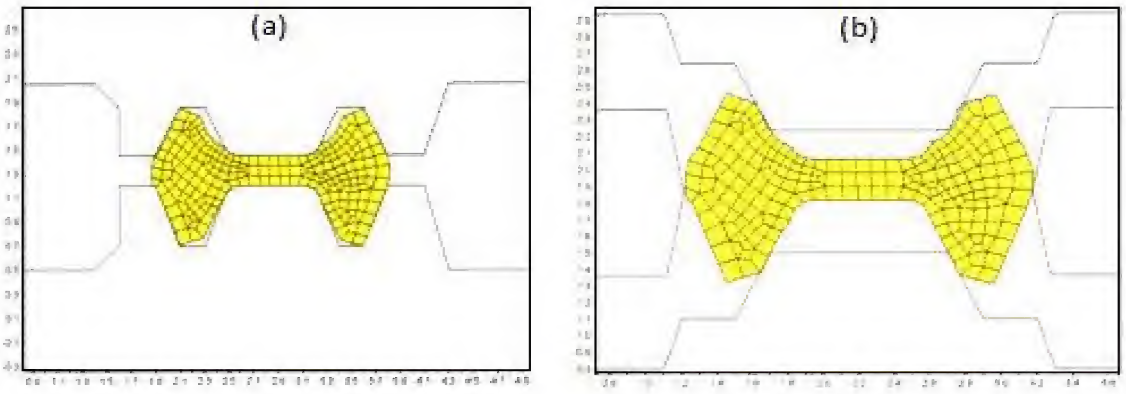

Figure 4: Simulation of Shape Rolling (a) Deformation after First Pass & (b) Setup for Second Pass

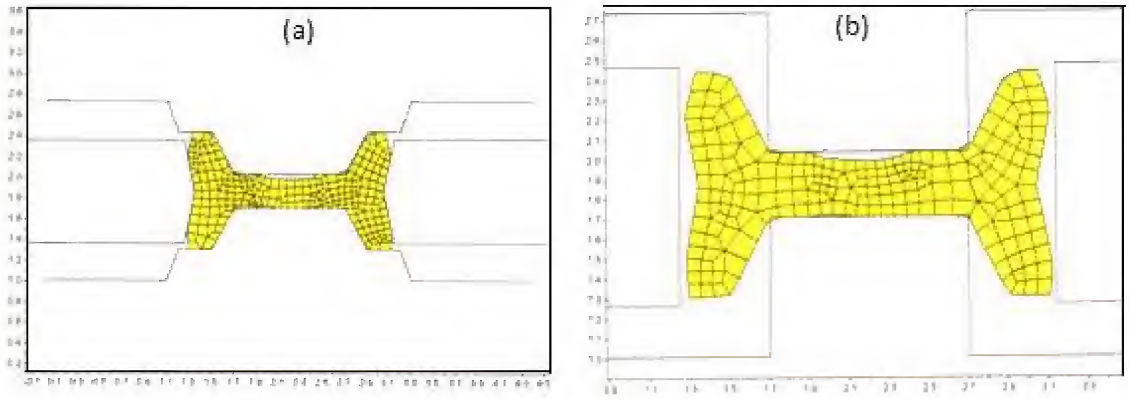

Figure 5: Simulation of Shape Rolling (a) Deformation after Second Pass & (b) Setup for Third Pass

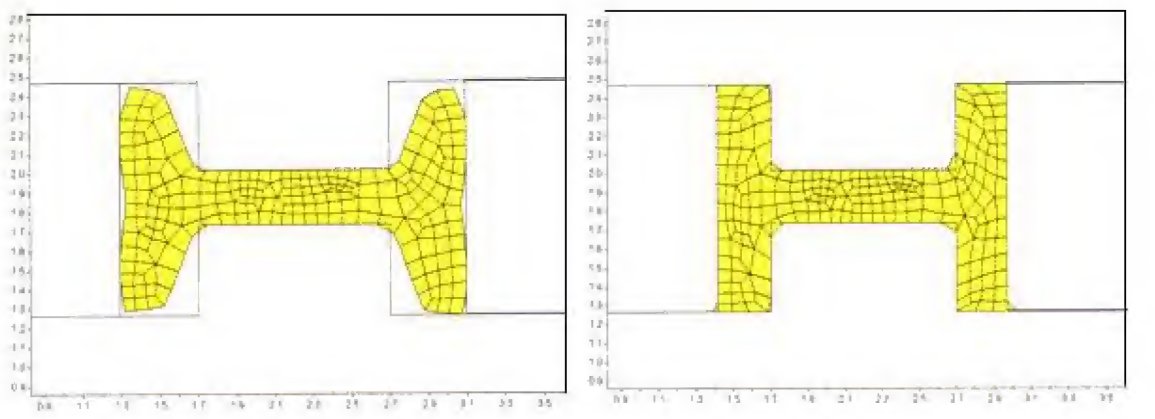

Figure 6: Simulation of Shape Rolling (a) Deformation after Third Pass & (b) After Fourth Pass

To achieve the desired shape of the product the working edges of the rollers are straightened as shown in figure 5b. The deformation shape after third pass is shown in figure 6a. This will be the setup for the final fourth pass. In this setup the position of upper and lower rollers is changed and they interfere with left and right rollers. The desire shape is obtained after fourth pass as shown in figure 6b.

RESULTS AND DISCUSSIONS

The results and discussion include the stresses and strains during different passes, metal flow during different passes, rolling force, and flow stress with variation strain.

Strain and Stress Induced During Different Passes of Shape Rolling

The effective strain and stress after first pass are shown in figure 7. It is quite clear that the connection area of the flange and web experiences highest strain during rolling. The maximum strain is 2.19 as shown in figure 7a. Figure 7b is the stress contour in the pressing direction of upper and lower rollers during the rolling process, which shows that the highest stress is located in the connection area of flange and web during rolling. The maximum stress is 389.17 MPa due to stress concentration at the corner connecting flange and web.

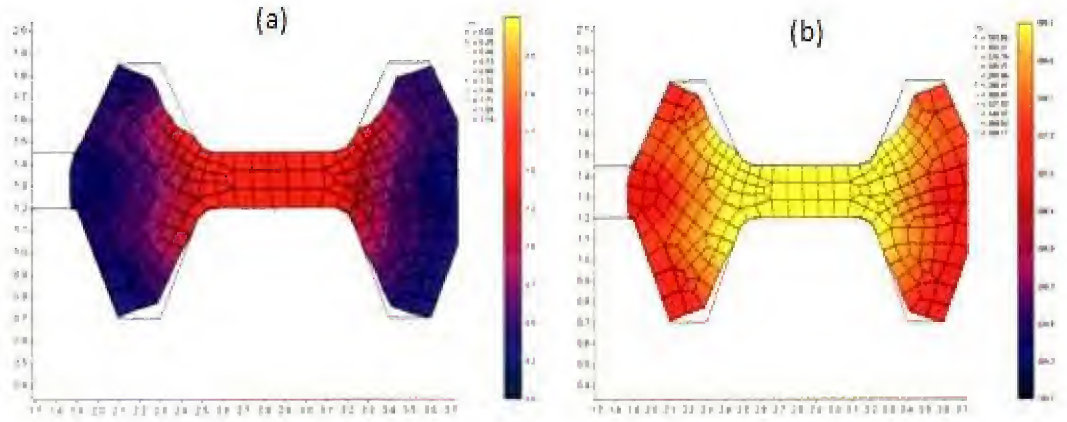

Figure 7: Effective Strain and Stress after First Pass (a) Stress and (b) Strain

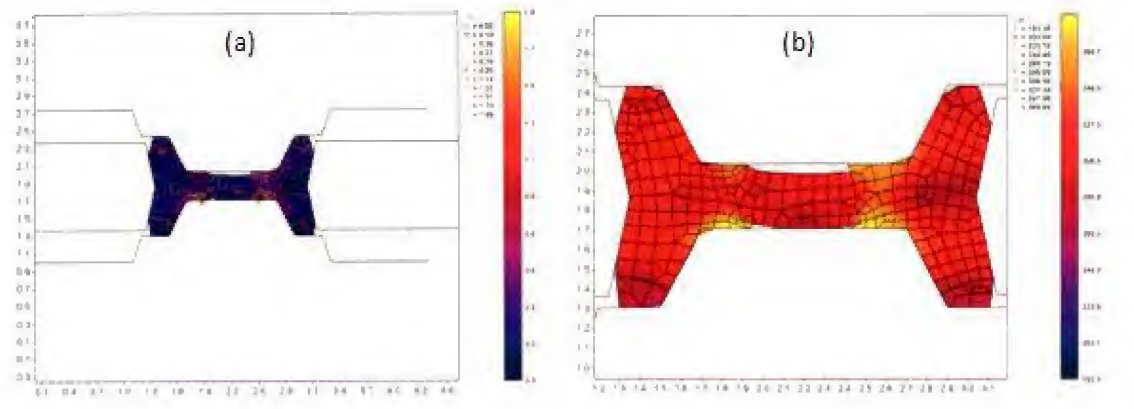

Figure 8: Effective Strain and Stress after Second Pass (a) Stress and (b) Strain

The effective strain and stress after second pass are shown in figure 8. For second pass the right roller moves leftward and left roller moves rightward. The rolling force was applied through flanges. The maximum strain of 1.89 was moved away from corner into the web region near corner of flange and web as shown in figure 6a. Figure 8b is the stress contour in the pressing direction of left and right rollers during the rolling process, which shows that the highest stress is located in the web region near to the corner. The maximum stress is 368.68 MPa due to stress concentration at the corner connecting flange and web. The strain and stress induced due to left and right rollers are less than those induced owing to upper and lower rollers.

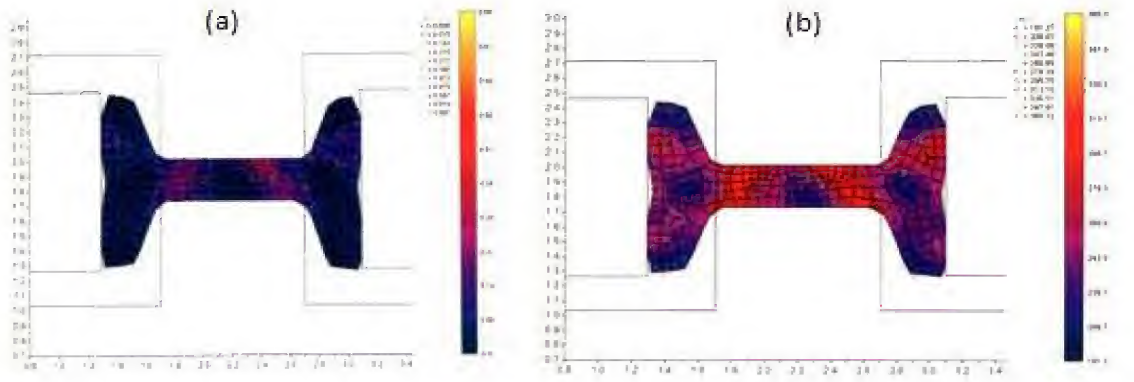

Figure 9: Effective Strain and Stress after Third Pass (a) Stress and (b) Strain

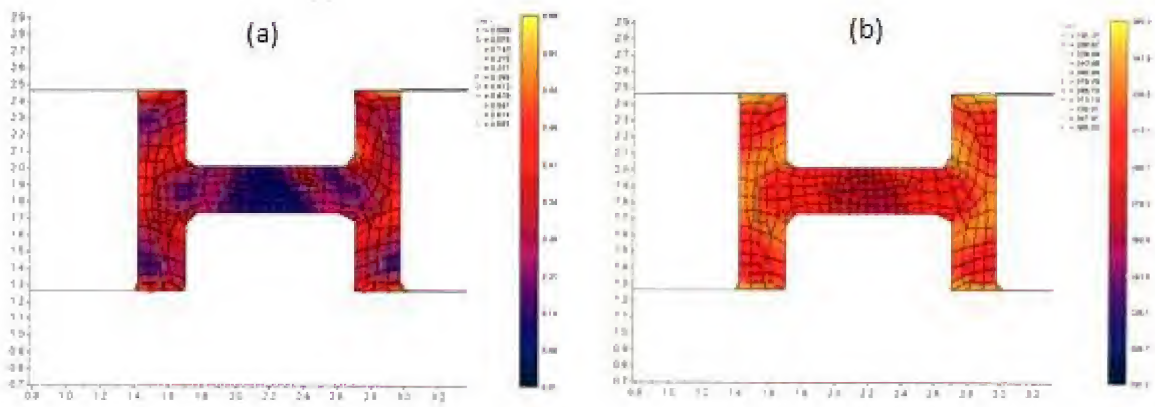

Figure 10: Effective Strain and Stress after Fourth Pass (a) Stress and (b) Strain

The effective strain and stress after third pass are shown in figure 9. For third pass all the rollers move simultaneously. The maximum strain was 0.681 and the maximum stress is 365.32 MPa. During this pass the straightening of flange and web takes place simultaneously in vertical and horizontal directions. Because of this straightening process, the induced stress and strain are less as compared first and second passes. The effective strain and stress after fourth pass are shown in figure 10. The straightening of flange and web and final shape of I-section is achieved in this fourth pass. The stress and strain are found to be equal to third pass.

Metal Flow during Different Passes of Shape Rolling

During the rolling of the H-beam, the status of metal flow in different parts determines final shape and dimension of the product. Figure 11a shows the metal flow during first pass. The displacement vector represents the metal flow in the flange stretching direction during rolling. It can be accomplished that the outer side of the flange flows toward top of the flange and the inner side of the flange flows toward the corner area of flange and web. Figure 11b shows the metal flow during third pass. The displacement vector represents the metal flow the top of the flange. The same phenomenon was observed during second pass also. Figure 12 shows the metal flow in the final pass. The displacement vector of metal flow shows that the vertical rollers obstruct the metal flow. The hindrance from the vertical roller leads to the reduction of forward slip zone, and the extension of backward slip zone. The horizontal rollers promote metal flow to straighten the flange.

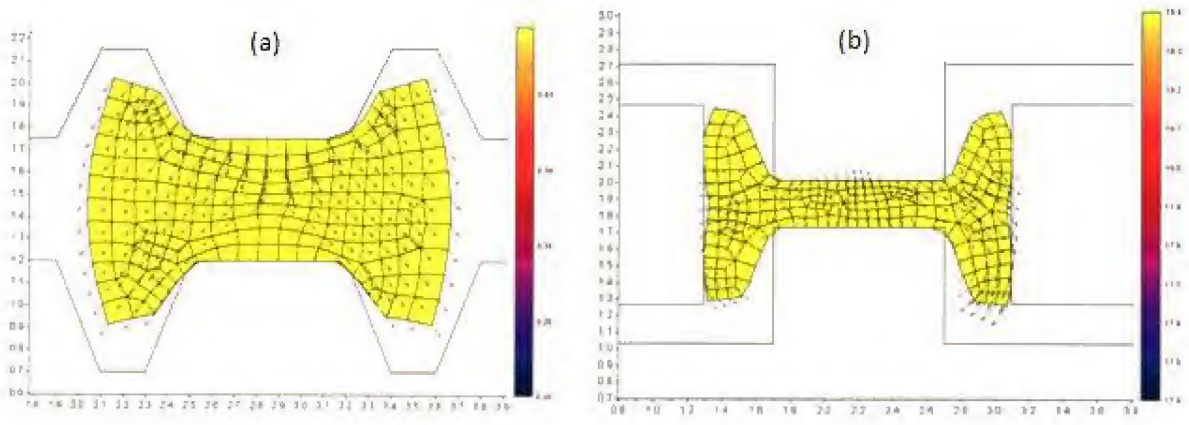

Figure 11: Metal flow during (a) First Pass and (b) Third Pass

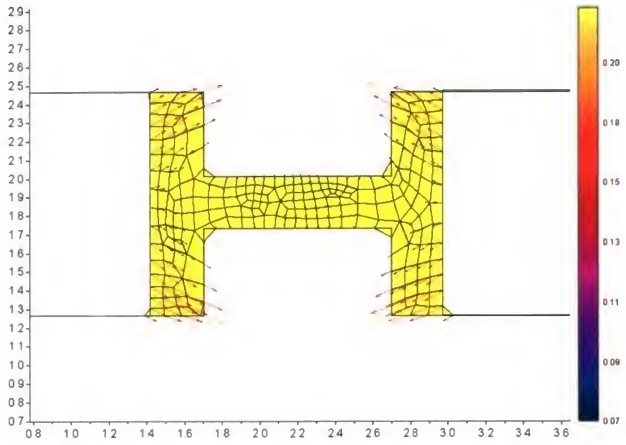

Figure 12: Metal Flow during Final Pass

Rolling Force

Figure 13 is the rolling force against at every instant of rolling process. It is observed that when the workpiece gets into the stable stage of rolling process, the rolling force is relatively steady. Figure 14 shows the variation of flow stress with strain. The curve represents the nature of plastic material with elastic region. The maximum stress induced in the material is lesser than allowable stress 390.20 MPA. The maximum strain is 2.0 which is greater than 1.89. The results obtained by simulation in comparison with material characteristic values are less and within limits. Hence, the design is safe. The simulation method gives good description of the processes and can be extended as a foundation of fundamental study or further research.

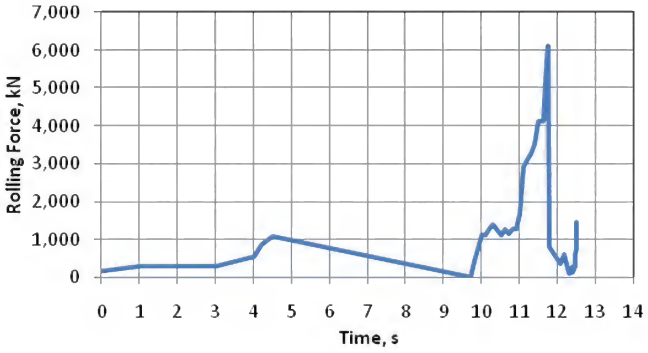

Figure 13: Variation of Rolling Force with Time

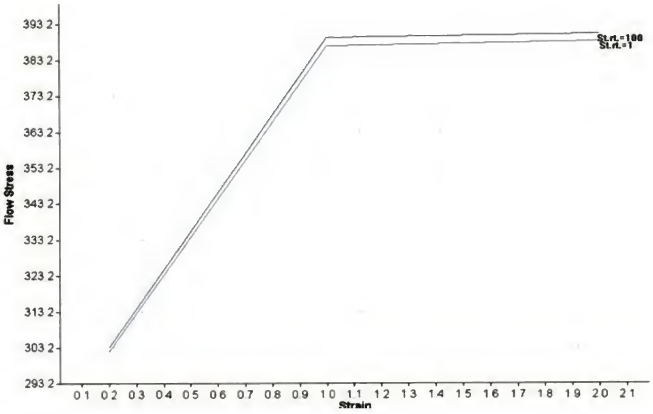

Figure 14: Variation of Flow Stress with Strain

CONCLUSIONS

The present work simulated the rolling process I –section beam, and studied the metal flow and the stress and strain field using DEFORM software. The maximum stress and strain induced in the material were respectively 389.17 MPa and 1.89 which were lesser than the material characteristic values. The stresses and strains induced during first pass are higher than during other passes. The results provide reliable references for the equipment checking and the process design.

ACKNOWLEDGEMENTS

The author thanks University Grants Commission (UGC), New Delhi for sponsoring this project for improving research activity in JNT University Hyderabad.

REFERENCES

1. Boljanovic & Vukota. (2009). Metal Shaping Processes. New York: Industrial Press. ISBN 978-0-8311-3380-1.
2. Chennakesava Reddy, A. (2006). Finite element analysis of reverse superplastic blow forming of Ti-Al-4V alloy for optimized control of thickness variation using ABAQUS, Journal of Manufacturing Engineering, 1, 6-9.
3. Chennakesava Reddy, A. (2012). Evaluation of local thinning during cup drawing of gas cylinder steel using isotropic criteria, International Journal of Engineering and Materials Sciences, 5. 71-76. DEFORM 2D Version 8.1.
4. Duggal, N, Ahmetoglu, M. A, Kinzel, G. L, & Altan, T. (1996). Computer aided simulation of cold roll forming a computer program for simple section profiles, Journal of Materials Processing Technology, 59, 41–48.
5. Heislitz, F, Livatyali, H, Ahmetoglu, M. A, Kinzel, G. L, & Altan, T. (1996). Simulation of roll forming process with the 3-D FEM code PAM-STAMP, Journal of Materials Processing Technology, 59, 59–67.
6. Kiuch, M, Koudabashi, T, & Eto, F. (1986). Development of simulation model of roll-forming processes. Journal of the Japan Society for Technology of Plasticity, 27, 874–881.
7. Onoda, Y, & Nagamachi, T. Finite element simulation of extroll forming process of heavy gauge square steel pipe. Journal of the Japan Society for Technology of Plasticity, 30, 1441–1446.
8. Wu W. T, Oh S. I, Altan T. & Miller R. A. (1990). Automated mesh generation for forming simulation. Proceedings of Computer Engineering conference, ASME, New York, **1**, 507.